White light wavefront control with a spatial light modulator

Dirk-Mathys Spangenberg,[1,*] **Angela Dudley**,[2] **Pieter H. Neethling**,[1] **Erich G. Rohwer**[1] **and Andrew Forbes**[1,2]

[1]*Stellenbosch University, Private Bag X1, Matieland 7602, South Africa*
[2]*CSIR National Laser Centre, PO Box 395, Pretoria 0001, South Africa*

dspan@sun.ac.za

Abstract: Spatial light modulators are ubiquitous tools for wavefront control and laser beam shaping but have traditionally been used with monochromatic sources due to the inherent wavelength dependence of the calibration process and subsequent phase manipulation. In this work we show that such devices can also be used to shape broadband sources without any wavelength dependence on the output beam's phase. We outline the principle mathematically and then demonstrate it experimentally using a supercontinuum source to shape rotating white-light Bessel beams carrying orbital angular momentum.

OCIS codes: (140.3300) Laser beam shaping; (050.0050) Diffraction and gratings; (050.4865) Optical vortices; (090.1995) Digital holography; (320.5540) Pulse shaping.

References and links

1. M. Padgett and R. Bowman, "Tweezers with a twist," Nat. Photon. **5**, 343–348 (2011).
2. K. Dholakia and T. Cizmar, "Shaping the future of manipulation," Nat. Photon. **5**, 335–342 (2011).
3. D. Grier, "A revolution in optical manipulation," Nature **424**, 810–816 (2003).
4. A. Jesacher, C. Maurer, A. Schwaighofer, S. Bernet and M. Ritsch-Marte, "Full phase and amplitude control of holographic optical tweezers with high efficiency," Opt. Express **16**, 4479–4486 (2008).
5. S. Ngcobo, I. Litvin, L. Burger and A. Forbes, "A digital laser for on-demand laser modes," Nat. Commun. **4**, 2289 (2013).
6. V. Arrizon, "Optimum on-axis computer-generated hologram encoded into low-resolution phase-modulation devices," Opt. Lett. **28**, 2521–2523 (2003).
7. C. Schulze, A. Dudley, D. Flamm, M. Duparre and A. Forbes, "Measurement of the orbital angular momentum density of light by modal decomposition," New J. of Physics **15**, 073025 (2013).
8. D. Flamm, C. Schulze, D. Naidoo, S. Schroter, A. Forbes and M. Duparre, "All-digital holographic tool for mode excitation and analysis in optical fibers," J. Lightwave Tech. **31**, 1023–1032 (2013).
9. D.W.K. Wong and G. Chen,"Redistribution of the zero order by the use of a phase checkerboard pattern in computer generated holograms," Appl. Opt. **47**(4), 602 (2008).
10. S. Furhapter, A. Jesacher, S. Bernet and M. Ritsch-Marte,"Spiral phase contrast imaging in microscopy," Opt. Express **13**, 689–694 (2005).
11. T. Feurer, Joshua C. Vaughan, Richard M. Koehl, and Keith A. Nelson. "Multidimensional control of femtosecond pulses by use of a programmable liquid-crystal matrix," Opt. Lett. **27**(8), 652 (2002)
12. E. Frumker and Y. Silberberg, "Femtosecond pulse shaping using a two-dimensional liquid-crystal spatial light modulator," Opt. Lett. **32**(11), 1384–1386 (2007).
13. E. Frumker and Y. Silberberg, "Phase and amplitude pulse shaping with two-dimensional phase-only spatial light modulators," J. Opt. Soc. Am. B **24**(12), 2940–2947 (2007).
14. J. C. Vaughan, T. Feurer, and K. A. Nelson. "Automated two-dimensional femtosecond pulse shaping," J. Opt. Soc. Am. B **19**(10), 2489 (2002).
15. J. C. Vaughan, T. Hornung, T. Feurer, and K. A. Nelson. "Diffraction-based femtosecond pulse shaping with a two-dimensional spatial light modulator," Opt. Lett. **30**(3), 323 (2005).
16. J. Leach and M. Padgett, "Observation of chromatic effects near a white-light vortex," New J. Phys. **5**, 154 (2003).

#208901 - $15.00 USD Received 27 Mar 2014; accepted 29 Apr 2014; published 30 May 2014

17. H. Sztul, V. Kartazayev and R. Alfano, "LaguerreGaussian supercontinuum," Opt. Lett. **31**, 2725-2727 (2006).
18. A. Wright, J. Girkin, G. Gibson, J. Leach and M. Padgett, "Transfer of orbital angular momentum from a supercontinuum, white-light beam," Opt. Express **16**, 9495-9500 (2008).
19. P. Fischer, H. Little, R.L. Smith, C. Lopez-Mariscal, C.T.A. Brown, W. Sibbett, and K. Dholakia, "Wavelength dependent propagation and reconstruction of white light Bessel beams," J. Opt. **8**, 477-482 (2006).
20. X. Zhu, A. Schulzgen, H. Wei, K. Kieu and N. Peyghambarian, "White light Bessel-like beams generated by miniature all-fiber device," Opt. Express **19**, 11365-11374 (2011).
21. A. Forbes, F. Dickey, M. DeGama and A. du Plessis, "Wavelength tunable laser beam shaping," Opt. Lett. **37**, 49–51 (2012).
22. J. Leach, G. Gibson, M. Padgett, E. Esposito, G. McConnell, A. Wright and J. Girkin, "Generation of achromatic Bessel beams using a compensated spatial light modulator," Opt. Express **14**, 5581-5587 (2006).
23. J. Morris, M. Mazilu, J. Baumgartl, T. Cizmar and K. Dholakia, "Propagation characteristics of Airy beams: dependence upon spatial coherence and wavelength," Opt. Express **17**, 13236-13245 (2009).
24. P. Fischer, C.T.A. Brown, J.E. Morris, C. Lopez-Mariscal, E.M. Wright, W. Sibbett, and K. Dholakia, "White light propagation invariant beams," Opt. Express **13**, 6657-6666 (2005).
25. R. Rop, A. Dudley, C. López-Mariscal and A. Forbes,"Measuring the rotation rates of superpositions of higher-order bessel beams," J. Mod. Opt., **59**, 259–267 (2012).
26. R. Vasilyeu, A. Dudley, N. Khilo and A. Forbes, "Generating superpositions of higher-order bessel beams," Opt. Express **17**, 23389–23395 (2009).

1. Introduction

Spatial light modulators (SLMs) are now standard tools for the shaping and control of light, having found applications in fields ranging from holographic optical trapping and tweezing [1–4], laser beam shaping and characterization [5–9] and imaging [10] to name but a few. These devices are primarily limited in two ways. First, the SLM has a finite range of phase change which it can introduce. This limit is usually compensated for by calibrating the device for a specific wavelength and then employing phase wrapping techniques. Second, SLMs cannot modify all the incident light, the extent of which depends on the type of SLM. This unmodulated light remains on-axis (at the optical center) and causes unwanted interference. To compensate for this unmodulated light a blazed grating is usually applied to the phase mask, thereby shifting the desired beam off-axis to the position of the first diffraction order of the blazed grating. Both compensation methods use phase wrapping, which is wavelength dependent. As such, SLMs have traditionally found use in applications where monochromatic sources are used. Yet spatial and temporal shaping of ultrafast lasers [11–15] and supercontinuum/white light sources [16–20] has become topical of late due to the numerous applications they have found. Various approaches have been explored to achieve this, often incorporating specialised optics such as prisms or diffractive elements [21–24] in conjuction with SLMs.

Here we outline how the aforementioned limitations of SLMs may in fact be used as self-compensating mechanisms to allow wavefront shaping of broadband light sources. We show mathematically that when operated in the first diffraction order with a blazed grating present, the SLM correctly shapes any wavelength of light, albeit at the expense of a reduced efficiency. We verify our model experimentally with a supercontinuum source before demonstrating the efficacy of the approach by controlling the rotation of white-light orbital angular momentum (OAM) carrying Bessel beams. Our results open new possibilities for the control of ultrafast, supercontinuum and other broadband sources with SLMs. We also offer a cautionary tale in how SLMs are calibrated as well as their use for temporal shaping of the spectral components of ultrafast lasers.

2. Mathematical model

In this section the known Fourier transform relations are used to investigate the effect of incorrect phase scaling on the SLM. SLMs are pixelated devices that allow one to change the relative phase of a wave incident at each pixel. For practical purposes the SLM is calibrated at a work-

#208901 - $15.00 USD Received 27 Mar 2014; accepted 29 Apr 2014; published 30 May 2014

ing wavelength (λ) such that the device linearly maps intensities selected by gray-levels, L, to phase shifts,ϕ, by $\phi(L) = 2\pi mL/256$ where $L \in [0..255]$ and $m \in \mathbb{N}$. This behaviour constitutes ideal or correct phase scaling. In order to formalize incorrect phase scaling we define a constant that denotes the difference between the actual and the ideal phase shift in the form of a ratio referred to as the difference constant, k_{d}. Incorrect phase scaling can therefore be expressed as, $\phi(L) = k_{\mathrm{d}}(L)2\pi mL/256$ where we have introduced a phase scaling function $k_{\mathrm{d}}(L)$ which is dependent on the selected gray-level, L. Constant incorrect phase scaling (CIPS) refers to the case where the phase scaling function is independent of the selected gray-level, $k_{\mathrm{d}}(L) = k_{\mathrm{d}}$. It is well-known that as with diffractive optical elements, the phase shift introduced by the SLM is dependent on wavelength through the dynamic phase shift $\Phi_{\mathrm{dyn}} = 2\pi nd/\lambda$, where n and d are the pixel refractive index and depth, respectively. The result is incorrect phase scaling at wavelengths other than the calibrated wavelength. If we assume the incorrect phase scaling is constant then k_{d} will only be dependent on wavelength. We will refer to working with a broadband source or at a different wavelength than the calibration wavelength collectively as working *off-wavelength*. Now we recall that the SLM is limited in that only a finite difference in phase may be applied between any two pixels. To overcome this limitation, phase wrapping is applied to the phase mask function, usually modulo 2π. The results we are about to show do not alter if another maximum phase value is selected. If working off-wavelength then CIPS occurs and the wrapping is done about $2\pi k_{\mathrm{d}}$. The value of k_{d} can easily be determined from $k_{\mathrm{d}} = \phi_{\mathrm{meas}}/\phi_{\mathrm{ideal}}$ where ϕ_{meas} and ϕ_{ideal} refer to the measured and ideal phase changes, respectively. When a blazed grating is added to the desired phase mask, CIPS affects this mask too. Here we show, for the first time, that when a blazed grating combined with some desired phase mask is affected by CIPS, one can use the spatial separation of orders caused by the blazed grating to compensate for the mismatch in phase, albeit at the expense of amplitude loss.

For the purpose of simplifying the following analysis we will consider only one dimensional phase mask functions with the understanding that the same principles apply when working in two dimensions. We begin with a generalized optical field described by,

$$f(x) \quad = \quad |f(x)| \exp(i\phi(x)), \tag{1}$$

which is multiplied by a linear phase gradient $g(x) = \exp(i\frac{2\pi}{p}x)$ to move the desired field away from the optical center. The linear phase gradient is chosen such that it would have a pitch p when wrapped around 2π. One can write an expression for the product $u(x)$ as,

$$u(x) = f(x) \times g(x) = |f(x)| \exp\left(i\left[\phi(x) + \frac{2\pi}{p}x\right]\right). \tag{2}$$

If one considers the effect of CIPS when $u(x)$ is wrapped about $2\pi k_{\mathrm{d}}$, then one can show (see Section 5.1) that the resulting field after wrapping is

$$u_{\mathrm{wr}}(x) \quad = \quad \sum_{n=-\infty}^{\infty} \mathrm{sinc}(\pi[n-k_{\mathrm{d}}])\,|f(x)| \exp\left(in\left[\phi(x) + \frac{2\pi}{p}x\right]\right), \tag{3}$$

where we have substituted $m = l = 1$ and $\Phi(x) = \phi(x) + \frac{2\pi}{p}x$ into Eq. 14 (see Section 5.1). The resultant equation, Eq. 3, can be reorganised more concisely as,

$$u_{\mathrm{wr}}(x) \quad = \quad \sum_{n=-\infty}^{\infty} \mathrm{sinc}(\pi[n-k_{\mathrm{d}}])\,|f(x)| \exp(in\phi(x)) \exp\left(i\frac{2\pi n}{p}x\right), \tag{4}$$

#208901 - $15.00 USD Received 27 Mar 2014; accepted 29 Apr 2014; published 30 May 2014

which can be Fourier transformed to find the expression in the spatio spectral domain,

$$U_{\mathrm{wr}}(X) = 2\pi \sum_{n=-\infty}^{\infty} \mathrm{sinc}(\pi[n-k_{\mathrm{d}}]) \times \Im\{|f(x)|\exp(in\phi(x))\} \circledast \delta\left(X - \frac{2\pi n}{p}\right). \quad (5)$$

From Eq. (5) one can make some interesting observations. It is evident that for each n a function exists, $|f(x)|\exp(in\phi(x))$, where its phase is independent of k_{d}. Further, the Fourier transform of this function will be shifted due to the applied phase gradient which results in a grating, by convolution with $\delta\left(X - \frac{2\pi n}{p}\right)$, to a spatial position which is dependant on the order n and the pitch p. It is clear that it is possible to separate the different order functions using a simple spatial filter. It can also be seen that k_{d} will determine the intensity of the diffraction orders according to $\mathrm{sinc}(\pi[n-k_{\mathrm{d}}])$. In other words, the holograms can be executed wavelength-independent if one is prepared to tolerate some intensity loss due to operating off-wavelength.

To illustrate the point, consider the usual case where a spatial filter is used to select only the first diffraction order, i.e., $n = 1$, and Eq. (2) is substituted into Eq. (5) with $A_1 = \mathrm{sinc}(\pi[1-k_{\mathrm{d}}])$,

$$\begin{aligned} U_{\mathrm{wr}}(X)|_{n=1} &= 2\pi A_1 \Im\{|f(x)|\exp(i\phi(x))\} \circledast \delta\left(X - \frac{2\pi}{p}\right) \\ &= 2\pi A_1 F\left(X - \frac{2\pi}{p}\right). \end{aligned} \quad (6)$$

It can be seen that the result is the Fourier transform of the desired (ideal) function but spatially shifted. We see that CIPS, in the first diffraction order of a blazed grating, does not affect the desired phase but rather the overall transmission intensity through the factor A_1. Note that the same can be said for higher orders, $n > 1$, since the phase function for higher orders is $\exp(in\phi(x))$.

3. Experimental methodology and results

We demonstrate that it is possible to do wavefront shaping with an SLM on broadband sources by first illustrating the wavelength dependent phase shift with a two-spot zero-order interference experiment. Following this, we show the wavelength independent phase shift with two additional experiments using the first diffraction order from a blazed grating. The experimental set-up is depicted in Fig. 1. In all three experiments a variable wavelength laser (Fianium supercontinuum SC400-4) was expanded through a $3\times$ telescope and directed towards a phase-only SLM (HoloEye, PLUTO-VIS, with 1920×1080 pixels of pitch 8 μm). The SLM was calibrated for a working wavelength of $\lambda = 715$ nm. The resulting optical fields, generated by either the physical mask [Fig. 1(a)] or the encoded holograms [Fig. 1(b) and 1(c)], were relay imaged through a spatial filtering set-up and then progated through a Fourier lens to observe the far field. Far field images were recorded with an objective lens and a camera (Logitec). Single wavelength and multi-wavelength measurements were made with (division 1 in red) and (division 2 in blue) respectively.

When performing phase measurements at single wavelengths (selected by an acousto-optic tunable filter within the source), the 4f imaging set-up (division 1) was implemented, while for the white light experiments this was replaced by the set-up shown in division 2. The latter was used to compensate for the angular dispersion caused by the blazed grating (since different wavelengths have a first order at differing angles). The compensation was achieved by encoding

#208901 - $15.00 USD Received 27 Mar 2014; accepted 29 Apr 2014; published 30 May 2014

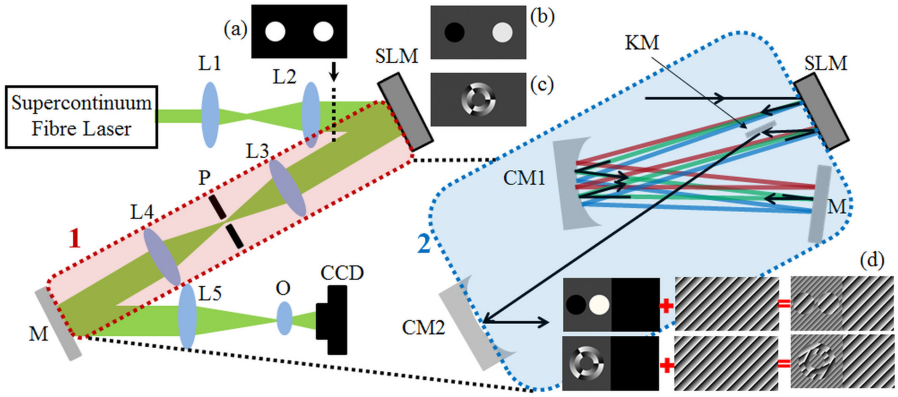

Fig. 1. Schematic of the experimental set-up [division 1 in red: imaging system for a single wavelength measurement; division 2 in blue: imaging system for a broadband wavelength measurement]. L: lens (f1 = 50 mm, f2 = 150 mm, f3 and f4 = 500 mm, f5 = 300 mm); SLM: spatial light modulator; P: pinhole; M: mirror; CM: curved mirror; KM: knife edge mirror; O: objective; CCD: camera. (a) The physical mask used to perform the two spot interference experiment without the blazed grating. The hologram encoded on the SLM for (b) the digital two spot interference experiment and (c) the annular ring interference experiment. (d) The holograms shown with the blazed grating encoded on the SLM to assist division 2 with the compensation of the lateral spatial dispersion for the broadband source.

identical blazed gratings on the desired hologram and the other half of the SLM, as depicted in Fig. 1(d). Light from one half of the SLM was relay imaged with a curved mirror (CM1) to the other half, where the imaging was done in the first diffraction order of the blazed grating. Thus the light dispersed from the first blazed grating was recombined by the second, such that the light exiting division 2 propagated in the same direction as that in division 1. In order to minimize chromatic aberration a curved mirror (CM2) was used to image the output from division 2 onto the camera. On a technical note we did not use a 90° staggered mirror after the curved mirror (CM1), and so a slight angular difference between the light coming from the blazed grating and that focussed back onto the second half of the SLM was observed. This caused the spectral components to propagate at slightly different angles when exiting the system, but for the purpose of the experiment this angular difference was deemed small enough to be acceptable.

3.1. Wavelength dependence

In the first experiment a physical mask, shown in Fig. 1(a), was inserted in the path of the beam as illustrated. The mask was orientated such that the light passing through each hole illuminated adjacent sectors of the SLM: one sector was programmed with a static gray-level, while the other cycled through a sequence of gray-levels from 0 to 255. The light from the SLM passed through a 4f imaging set-up indicated by division 1, with the pinhole (P) removed. The interference patterns captured by the camera were analysed to determine the phase shift introduced by the SLM for each gray-level setting, with the results shown in Fig. 2.

In Fig. 2(a) we see that the measured phase shift scales linearly with the selected gray-level; therefore CIPS applies and we may use our analysis from Section 2. From this data we find that the ratio between the selected gray-level and the measured phase shift is independent of the

#208901 - $15.00 USD Received 27 Mar 2014; accepted 29 Apr 2014; published 30 May 2014

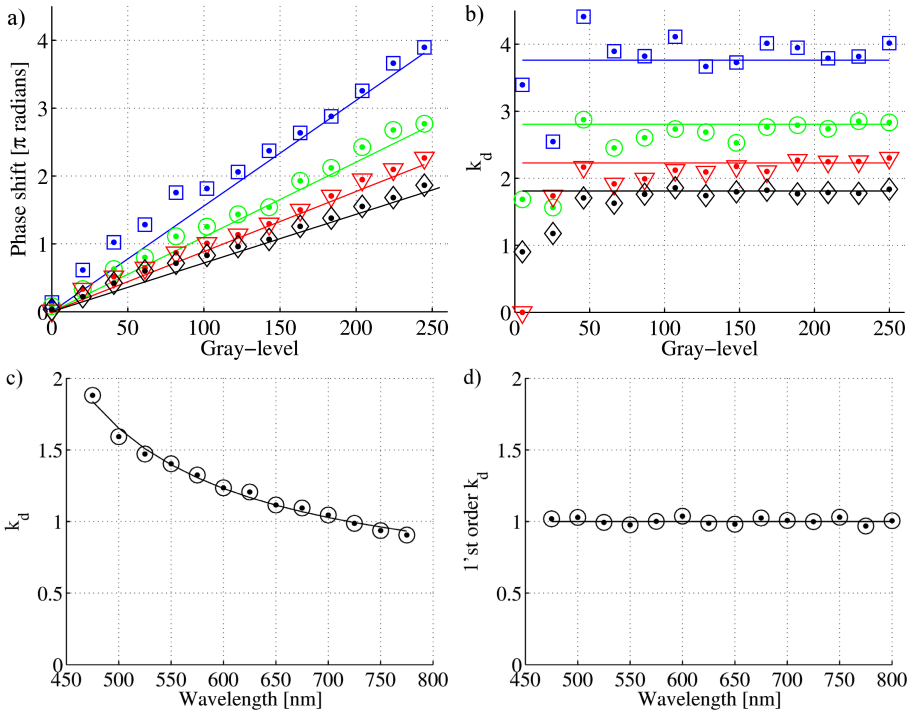

Fig. 2. (a) The measured phase shift plotted against the gray-level for different wavelengths (blue: 475 nm; green: 550 nm; red: 650 nm and black: 775 nm). (b) The ratio between the measured and ideal phase (k_{d}) plotted against the gray-level. (c) The ratio between the measured and ideal phase (k_{d}) for various wavelengths for the physical mask and (d) the two spot hologram in the first diffraction order.

selected gray-level, i.e., $k_{\mathrm{d}}(L,\lambda) = k_{\mathrm{d}}(\lambda)$, as shown in Fig. 2(b). The wavelength dependence of $k_{\mathrm{d}}(\lambda)$ in the zero diffraction order can clearly be seen in Fig. 2(c). These results confirm the well-known wavelength dependence of SLMs.

3.2. Wavelength independence

In the second experiment the physical mask was removed and the beam was directed onto the SLM which was encoded, via complex amplitude modulation [9], with two spots [as shown in Fig. 1(b)]. One spot was programmed with a static gray-level, while the other cycled through a sequence of gray-levels from 0 to 255, thus mimicking the physical mask in the previous experiment, but implemented digitally and with the addition of a blazed grating. The light from the SLM then passed through a 4f imaging set-up indicated by divisions 1 and 2 in Fig. 1 for the single and off-wavelength measurements, respectively. By considering the interference of the two plane waves (assigned by each of the spots) and introducing a phase shift in one of the waves (due to the gray-level change in the second spot), a shift in the position of the interference fringes was observed. This shift was measured and is depicted in Figs 3(a) and 3(b) for a single wavelength ($\lambda = 532$ nm) and the broadband source, respectively. Accompanying videos of the interference fringes moving as the gray-level varies are presented as inserts. In Fig. 3(a) it is evident that the interference fringes shift linearly in agreement with the encoded gray-level. The measurements for the broadband source, shown in Fig. 3(b), confirms that when a

#208901 - $15.00 USD Received 27 Mar 2014; accepted 29 Apr 2014; published 30 May 2014

blazed grating is added the CIPS due to the hologram (i.e. the two-spot hologram) and the blazed in combination with wrapping spreads the resultant orders such that no undesired phase modulation results in the first order as a function of wavelength. Analysis of this data is shown in Fig. 2(d), alongside the previous data in Fig. 2(c). The results offer compelling evidence that wavalength independent wavefront control is possible when operating in the first order with a blazed grating since $k_{\mathrm{d}} = 1$ for all wavelengths.

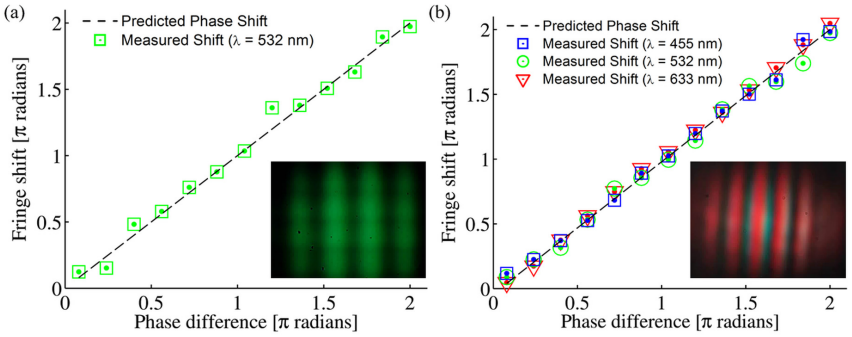

Fig. 3. The measured interference fringe shift plotted against the encoded phase difference for (a) a single wavelength ($\lambda = 532$ nm) and (b) the broadband source. Corresponding videos illustrating the shift in the interference pattern can be viewed as (Media 1) and (Media 2), respectively.

3.3. Rotating white-light Bessel beams

Finally, we apply the concept for the arbitrary shaping of a supercontinuum beam. We repeat previous experiments that were performed using monochromatic sources with our supercontinuum beam. As an example we consider the creation and rotation of superpositions of higher-order Bessel beams carrying orbital angular momentum [25,26]. This calls for control of the azimuthal phase, phase velocity and amplitude distribution of the fields and in this sense is a good example of a general problem. The required holograms take the form of two ring-slits, each possessing an azimuthal phase of equal order but opposite handedness ($l_1 = +3$ and $l_2 = -3$) as shown in Fig. 1(c). The holograms can be defined by the following transmission function

$$t(r,\phi) = \begin{cases} \exp(il\phi) & \text{if } R \geq r \geq R-\Delta \\ \exp(-il\phi)\exp(i\varphi) & \text{if } R \leq r \leq R+\Delta \end{cases}, \tag{7}$$

where l is the azimuthal index, ϕ the azimuthal angle, φ the phase difference introduced in the outer ring-slit, R the radius of the two ring-slits and Δ their widths. The amplitude of the resulting optical field, observed in the far field, is defined as

$$u(r,\phi) \quad = \quad J_l(r)\exp(il\phi) + J_{-l}(r)\exp(-il\phi)\exp(i\varphi), \tag{8}$$

where $J_l(r)$ denotes the l-th order Bessel function. When the orders, $|l|$, of the two azimuthal phases are equal but of opposite handedness, a "petal" structure is produced, where the number of petals is denoted by $2|l|$. These non-diffracting petal-like modes rotate as they propagate and have been studied in detail elsewhere [25, 26]. A phase difference between the two annular rings was varied between 0 and 2π, resulting in a rotation of the interference (or petal) pattern, which was measured by observing the angular displacement of the petals. This angular displacement (or rotation) was measured and is depicted in Figs 4(a) and 4(b) for a single

#208901 - $15.00 USD Received 27 Mar 2014; accepted 29 Apr 2014; published 30 May 2014

wavelength ($\lambda = 532$ nm) and the broadband source, respectively. Accompanying videos of the petals rotating as the gray-level varies are presented as inserts. In Fig. 4(a) it is evident that the petals rotate linearly in agreement with the encoded gray-level. The measurements for the broadband source contained in Fig. 4(b) also show that the rotation rate is linear in agreement with the encoded gray-level, confirming that no undesired phase modulation occurs as a function of the wavelength.

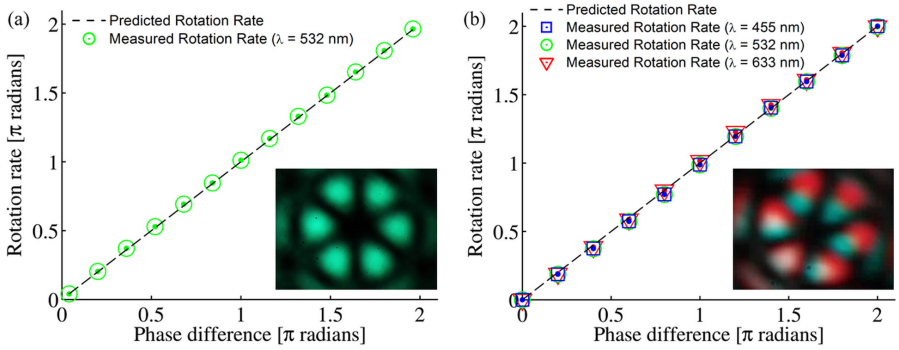

Fig. 4. The measured petal rotation rate plotted against the encoded phase difference for (a) a single wavelength ($\lambda = 532$ nm) and (b) the broadband source. Corresponding videos illustrating the rotation in the interference pattern can be viewed as (Media 3) and (Media 4), respectively.

4. Conclusion

We have derived mathematically an expression which describes the decomposition of an input function when CIPS is present. The mathematical model shows that the phase function is separated into orders, each of which scale linearly by the order number. We have shown experimentally that the resultant phase function behaves ideally in the first order when working at wavelengths different to the calibration wavelength. We have shown that broadband spatial beam shaping is possible if a reduction in efficiency can be tolerated. This result also has implications for set-ups utilising 2D SLMs to do temporal shaping where the efficiency of the first order of blazed diffraction gratings are modified to change the amplitude of spectral components [15].

There is an important corollary to this work that takes its impact beyond that of shaping broadband sources: the influence of calibration on SLM performance. Our results suggest that good results in the first diffraction order do not imply a well calibrated device, since the first order, when operated with a blazed grating, will always produce the correct results. As an outlook, we note that these results should extrapolate to any periodic phase grating, which would imply that if optical efficiency is not a concern, then calibration of the SLM may not even be necessary.

5. Appendix Mathematical model

In this appendix Fourier transform analysis is used to investigate the effect of phase wrapping about $2\pi l k_{\mathrm{d}}$ due to CIPS, where $l \in \mathbb{N}$. We also show that the general form of the blazed grating can be decomposed into the sum of weighted linear phase gradients.

#208901 - $15.00 USD Received 27 Mar 2014; accepted 29 Apr 2014; published 30 May 2014

5.1. *Constant incorrect phase scaling (CIPS) and phase wrapping*

CIPS occurs when one has a constant scaling factor k_{d} which is multiplied by all phase values in an input phase function. This results in non-ideal phase wrapping. The ideal wrapping value for a phase mask function is $2\pi l$ therefore non-ideal wrapping is done about a phase $2\pi l k_{\mathrm{d}}$.

Below CIPS is taken into account for any phase function when non-ideal wrapping is applied. If one considers a complex valued input function as the sum of point sources given by,

$$\begin{aligned} f(x) = |f(x_1)|\,\mathrm{e}^{ik_{\mathrm{d}}\Phi_1}\delta(x-x_1) + |f(x_2)|\,\mathrm{e}^{ik_{\mathrm{d}}\Phi_2}\delta(x-x_2) \\ + |f(x_3)|\,\mathrm{e}^{ik_{\mathrm{d}}\Phi_3}\delta(x-x_3) + \ldots, \end{aligned} \tag{9}$$

then each point source could be expanded such that it takes the form of a linear phase gradient as follows,

$$|f(x_m)|\,\mathrm{e}^{ik_{\mathrm{d}}\Phi_m}\delta(x-x_m) \quad = \quad |f(x_m)|\,\mathrm{e}^{\frac{ik_{\mathrm{d}}\Phi_m}{x_m}x}\delta(x-x_m), \text{ where } m \in \mathbb{N}. \tag{10}$$

When wrapping is applied about the position $\theta = 2\pi l k_{\mathrm{d}}$ a pitch p can be calculated for the linear phase gradient given by $\mathrm{e}^{i\frac{k_{\mathrm{d}}\Phi_m}{x_m}x}$ in Eq. 10 as,

$$p \quad = \quad \frac{2\pi l x_m}{\Phi_m}. \tag{11}$$

Now using the result from section 5.2, Eq. 16, one can express the linear phase for each point source, given by $\mathrm{e}^{i\frac{k_{\mathrm{d}}\Phi_m}{x_m}x}$ in Eq. 10, as a wrapped phase gradient about the point $\theta = 2\pi l k_{\mathrm{d}}$,

$$g\left(x, 2\pi l k_{\mathrm{d}}, \frac{2\pi l x_m}{\Phi_m}\right) \quad = \quad \sum_{n=-\infty}^{\infty} \mathrm{sinc}\left(\pi\left[n - l k_{\mathrm{d}}\right]\right)\mathrm{e}^{i\frac{n\Phi_m}{lx_m}x}. \tag{12}$$

From the above method one can write an expression for the initial function given by Eq. 9, when wrapping about $2\pi l k_{\mathrm{d}}$ is applied, by substituting all the phase constants with the wrapped equation given by Eq. 12 to find the wrapped expression of the function,

$$\begin{aligned} f_{\mathrm{wr}}(x) = \sum_{n=-\infty}^{\infty} \mathrm{sinc}\left(\pi\left[n - l k_{\mathrm{d}}\right]\right)\Big[|f(x_1)|\,\mathrm{e}^{i\frac{n}{l}\Phi_1}\delta(x-x_1) + |f(x_2)|\,\mathrm{e}^{i\frac{n}{l}\Phi_2}\delta(x-x_2) \\ + |f(x_3)|\,\mathrm{e}^{i\frac{n}{l}\Phi_3}\delta(x-x_3) + \ldots\Big], \end{aligned} \tag{13}$$

which one can simplify to,

$$f_{\mathrm{wr}}(x) \quad = \quad |f(x)| \sum_{n=-\infty}^{\infty} \mathrm{sinc}\left(\pi\left[n - l k_{\mathrm{d}}\right]\right)\mathrm{e}^{i\frac{n}{l}\Phi(x)}. \tag{14}$$

Thus one can see that the function when wrapped becomes the amplitude of the function multiplied by the sum of weighted whole number multiples of the phase of the function and we have derived a simple way to apply wrapping to any input function.

5.2. *Wrapping of a linear phase gradient.*

Given a linear phase gradient $\mathrm{e}^{i\frac{\theta}{p}x}$ wrapped around a phase of θ such that the resultant sections have a pitch p, see Fig. 5, which can be written as a composition of functions,

$$g(x) \quad = \quad \mathrm{e}^{i\frac{\theta}{p}x}\mathrm{rect}\left(\frac{2}{p}x\right) \circledast \sum_{n=-\infty}^{\infty} \delta(x - np).$$

#208901 - $15.00 USD Received 27 Mar 2014; accepted 29 Apr 2014; published 30 May 2014

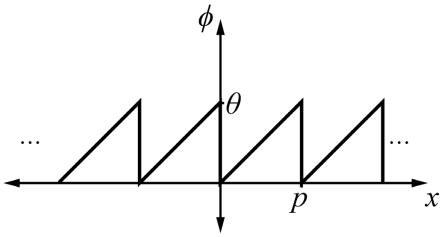

Fig. 5. Cross-section view of a linear phase gradient wrapped around a phase of θ with sections spaced with a pitch p.

The Fourier transform of $g(x)$ can be derived and simplified,

$$\begin{aligned} G(X) &= 2\pi\delta\left(X-\frac{\theta}{p}\right) \circledast \operatorname{sinc}\left(\frac{p}{2}X\right) \times \sum_{n=-\infty}^{\infty} \delta\left(X-\frac{2\pi n}{p}\right) \\ &= 2\pi\operatorname{sinc}\left(\frac{p}{2}\left[X-\frac{\theta}{p}\right]\right) \times \sum_{n=-\infty}^{\infty} \delta\left(X-\frac{2\pi n}{p}\right) \\ &= 2\pi \sum_{n=-\infty}^{\infty} \operatorname{sinc}\left(\frac{p}{2}\left[\frac{2\pi n}{p}-\frac{\theta}{p}\right]\right) \delta\left(X-\frac{2\pi n}{p}\right) \\ &= 2\pi \sum_{n=-\infty}^{\infty} \operatorname{sinc}\left(\pi\left[n-\frac{\theta}{2\pi}\right]\right) \delta\left(X-\frac{2\pi n}{p}\right). \end{aligned} \tag{15}$$

Using the inverse Fourier transform one can express the resultant equation, Eq. 15, as,

$$g(x,\theta,p) = \sum_{n=-\infty}^{\infty} \operatorname{sinc}\left(\pi\left[n-\frac{\theta}{2\pi}\right]\right) \mathrm{e}^{i\frac{2\pi n}{p}x}. \tag{16}$$

Thus we have shown that,

$$\mathrm{e}^{i\frac{\theta}{p}x}\operatorname{rect}\left(\frac{2}{p}x\right) \circledast \sum_{n=-\infty}^{\infty} \delta(x-np) = \sum_{n=-\infty}^{\infty} \operatorname{sinc}\left(\pi\left[n-\frac{\theta}{2\pi}\right]\right) \mathrm{e}^{i\frac{2\pi n}{p}x},$$

which means one can express any wrapped linear phase gradient as the weighted sum of linear phase gradients.

#208901 - $15.00 USD Received 27 Mar 2014; accepted 29 Apr 2014; published 30 May 2014